Int J Fract (2009) 160:109–118
DOI 10.1007/s10704-009-9399-3

ORIGINAL PAPER

Multiscale continuum modeling of a crack in elastic media with microstructures

G. L. Huang · C. T. Sun

Received: 1 November 2008 / Accepted: 10 September 2009 / Published online: 6 November 2009

Abstract Cosserat type continuum theories have been employed by many authors to study cracks in elastic solids with microstructures. Depending on which theory was used, different crack tip stress singularities have been obtained. In this paper, a microstructure continuum theory is used to model a layered elastic medium containing a crack parallel to the layers. The crack problem is solved by means of the Fourier transform. The resulting integrodifferential equations are discretized using the Chebyshev polynomial expansion method for numerical solutions. By using the present theory, the explicit internal length effects upon the crack opening displacement and stress field can be observed. It is found that the stress field near the crack tip is not singular according to the microstructure continuum solution although the level of the opening stress shows an increasing trend until it gets very close to the crack tip. The rising portion of the near tip opening stress is used to project the stress intensity factor which agrees fairly well with that obtained using the FEM to perform stress analyses of the cracked layered medium with the exact geometry. The numerical solutions also indicate that treating the layered medium as an equivalent homogeneous classical elastic solid is not adequate if cracks are present and accurate stress intensity factors in the original layered medium is desired.

Keywords Microstructure continuum · Layered medium · Crack · Stressintensity factor · Fourier transform

G. L. Huang
Department of Systems Engineering, University of Arkansas at Little Rock, Little Rock, AR 72204, USA

C. T. Sun (✉)
School of Aeronautics and Astronautics, Purdue University, West Lafayette, IN 47907, USA
e-mail: sun@purdue.edu

1 Introduction

The use of continuum approach for modeling solids has been practiced by both engineers and scientists successfully for hundreds of years. For obvious reasons, the conventional continuum models are efficient for modeling macro scale solids but may not be efficient and accurate in describing microstructural effects. One alternative to solving the above mentioned problem is to employ additional kinematic variables to describe the nonhomogeneous local deformation in the microstructure. Cosserat and Cosserat (1909) first proposed a nonclassical continuum. Following that, many other forms were proposed such as the couple stress theory by Toupin (1962), the microstructure theory by Mindlin (1964), and the micromorphic theory by Eringen and Suhubi (1964), the strain gradient theory (Fleck and Hutchinson 1993; Aifantis 1999). Common to all these theories is the adoption of a generic configuration of the microstructure from which the equations of motion and general constitutive equations are developed. The constitutive equations are expressed in general forms leaving many material constants to be determined by very

prohibitive experiments. Another group of researchers took a slightly different approach in deriving microstructure continuum theories by taking into account specific geometries of the microstructure. Both global displacements and additional kinematic variables are introduced to describe the motion and deformation of the material unit cell containing the microstructure. Such an approach was first proposed by Sun et al. (1968) and Achenbach et al. (1968) for periodically layered media. The main advantage of this approach is that the constitutive relations are derived explicitly from the properties and configuration of the microstructure and no additional testing of material properties is necessary. Moreover, the explicit internal characteristic length effects can also be captured with this formulation.

All the Cosserat and Cosserat (1909) type nonconventional continuum theories have to adopt certain simplifying assumptions regarding the local deformation in the microstructure. As a result, their ability in describing the local deformation and stress fields in the microstructure is often questioned. Moreover, some solutions to the same physical problem obtained using different Cosserat and Cosserat (1909) type continuum theories are expressed in quite different mathematical forms and can be quite different from the solution based on the classical continuum theory. For instance, a number of Cosserat and Cosserat (1909) continuum theories have been employed to study crack problems with the result of various crack tip stress singularities. Sternberg and Muki (1967) first studied the stress field around a mode I crack by using the couple-stress theory in conjunction with the Fourier transform approach. They concluded that near tip fields in an elastic material are governed by the Cauchy stress and the couple stress with $O(r^{-1/2})$ and $O(r^{-3/2})$ singularities, respectively, at the crack tip. Similar conclusions have been obtained by Atkinson and Leppington (1977) and by Paul and Sridharan (1981) for the mode I crack by using the couple-stress theory with the aid of the Wiener-Hopf method. Eringen et al. (1977) used the non-local theory to study the state of stress near a sharp line crack in an elastic plane subjected to uniform tension, shear and anti-plane shear loadings. According to this (non-local) theory, stress singularity around the crack tip vanishes. As a result, it was suggested that the maximum stress at the crack tip be used as a fracture criterion. Kennedy and Kim (1993) studied a stationary finite crack subjected to a dynamic load using the micropolar elasticity and found that materials with strong micropolar properties have significantly lower dynamic energy release rates than their classical elastic solid counterparts. Because of its simplicity, the strain gradient theory has recently been used to interpret microstructural effects found in fracture problems. Huang et al. (1997) studied the near tip fields for mixed mode cracks. Based on their results, both the Cauchy stress and couple stress fields have the inverse square root singularity near the crack tip. Zhang et al. (1998) studied the mode III crack problem by using the couple-stress theory and found $O(r^{-3/2})$ stress singularity at the crack tip. On the other hand, Vardoulakis et al. (1996) considered a mode III crack in a strain gradient continuum theory with or without a surface energy and obtained a different stress singularity $O(r^{-1/2})$. Fannjiang et al. (2002) studied a mode III finite crack using a strain gradient elasticity. They illuminated the transition from the strain gradient theory to the classical elasticity theory as intrinsic lengths vanish.

In the works cited above, no attempt has been made to compare the crack opening stresses near the crack tip obtained from Cosserat type continuum theories and the exact solution based on the exact layered geometry. Consequently, the significance of the various stress singularities predicted by the Cosserat type models cannot be evaluated. In this paper, we employ a microstructure continuum theory to investigate crack problems in an elastic layered medium. The crack is assumed to be parallel to the plane of the layers. The layered medium is modeled as a microstructure continuum for which the solution for the crack problem is solved by means of the Fourier transform. The results obtained from the microstructure continuum theory are compared with those obtained with the effective modulus theory and the finite element analysis of the layered medium with the exact geometry.

2 A microstructure continuum theory for layered media

The formulation of the microstructure continuum theory for layered media developed by Sun et al. (1968) and Achenbach et al. (1968) is briefly reviewed. Details of the derivation can be found in these two references. Consider a layered medium consisting of a large number of alternating plane, parallel layers of two homogeneous, isotropic elastic materials, as shown in Fig. 1. The Lamé constants, mass densities, and thicknesses

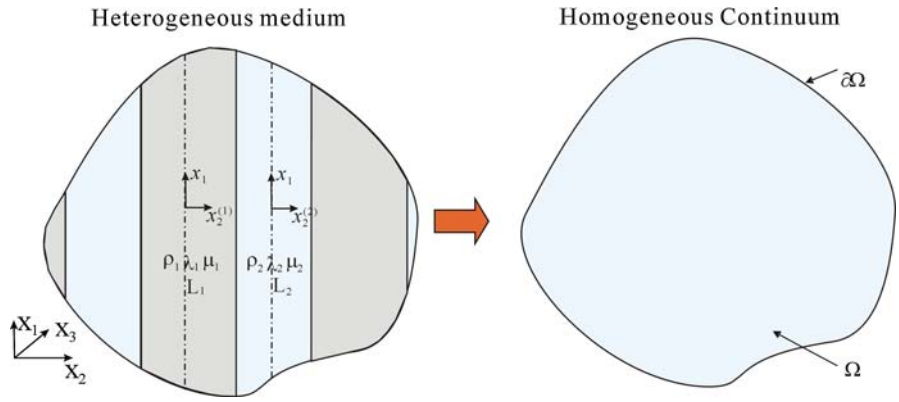

Fig. 1 A heterogeneous solid replaced by a homogeneous solid with microstructures

of layers 1 and 2 are denoted as λ_j, μ_j, ρ_j and $L_j (j = 1, 2)$, respectively. Two local coordinate systems $(x_1, x_2^{(1)}, x_3)$ and $(x_1, x_2^{(2)}, x_3)$ are defined with axes parallel to the global coordinates $X_i (i = 1, 2, 3)$ and with origins in the midplanes of the individual layers, respectively. The displacements in the midplanes are denoted as $u_{0i}^{(1)}$ and $u_{0i}^{(2)}$ for layers 1 and 2, respectively. The subscript $i = 1, 2, 3$ represents the displacement component along the x_i direction, and superscripts (1) and (2) represent layers 1 and 2, respectively.

Consider a representative volume element (RVE) consisting of a pair of layers 1 and 2 with as with total cell length $L = L_1 + L_2$. Assume a plane strain state parallel to the $X_1 - X_2$ plane. If the characteristic length of deformation is not too small compared with the thicknesses of the layers, the local displacements in the layers can be approximated with linear series expansions with respective to the local coordinates as

$$u_i^{(1)} = u_{0i}^{(1)}(X_2) + \phi_{2i}^{(1)}(X_2) x_2^{(1)} \tag{1}$$

$$u_i^{(2)} = u_{0i}^{(2)}\left(X_2 + \frac{L}{2}\right) + \phi_{2i}^{(2)}(X_2) x_2^{(2)} \tag{2}$$

where the kinematic variables $\phi_{ji}^{(\alpha)}(X_k)(\alpha = 1, 2)$ are the first order expansion functions that describe the micro deformation field in layer α. The displacement continuity condition at the interface between the two layers is given by

$$u_{0i}^{(1)}\left(X_2 + \frac{L}{2}\right) - u_{0i}^{(1)}(X_2) = \phi_{2i}^{(1)}(X_2)\frac{L_1}{2} + \phi_{2i}^{(2)}(X_2)\frac{L_2}{2} \tag{3}$$

To eliminate $\phi_{2i}^{(2)}$ through Eq. (3) and the potential energy density W of the macro-homogeneous medium can be expressed in terms of $U_i(X_k) \equiv u_{0i}^{(1)}$, $\Phi_{ji} \equiv \phi_{ji}^{(1)}$ and their derivatives, which are functions of the global coordinates. By defining the conventional strain e_{ij} in terms of the displacement U_i as

$$e_{ij} = \frac{1}{2}\left(\frac{\partial U_j}{\partial X_i} + \frac{\partial U_i}{\partial X_j}\right), \tag{4}$$

the relative deformation

$$\gamma_{ij} = \frac{\partial U_j}{\partial X_i} - \Phi_{ij} \tag{5}$$

with $\gamma_{ij} = 0$ for $i \neq 2$, the gradient of the relative deformation

$$\theta_{kij} = \frac{1}{2}\left(\frac{\partial \gamma_{ij}}{\partial X_k} + \frac{\partial \gamma_{ik}}{\partial X_j}\right) \quad \text{for } k, j = 1, 3 \tag{6}$$

$$\theta_{kij} = \frac{\partial \gamma_{ij}}{\partial X_k} \quad \text{otherwise.} \tag{7}$$

Based on the Hamilton's principle, the displacement equations of motion can be obtained as

$$a_1\frac{\partial^4 U_1}{\partial X_1^2 \partial X_2^2} + a_2\frac{\partial^2 U_1}{\partial X_1^2} + a_3\frac{\partial^2 U_1}{\partial X_2^2} + a_4\frac{\partial^2 U_2}{\partial X_1 \partial X_2} + a_5\frac{\partial^3 \Phi_{21}}{\partial X_1^2 \partial X_2} + a_6\frac{\partial \Phi_{21}}{\partial X_2} + a_7\frac{\partial \Phi_{22}}{\partial X_1} = 0 \tag{8}$$

$$a_8\frac{\partial^4 U_2}{\partial X_1^2 \partial X_2^2} + a_9\frac{\partial^2 U_2}{\partial X_1^2} + a_{10}\frac{\partial^2 U_2}{\partial X_2^2} + a_4\frac{\partial^2 U_1}{\partial X_1 \partial X_2} + a_{11}\frac{\partial \Phi_{21}}{\partial X_1} + a_{12}\frac{\partial^3 \Phi_{22}}{\partial X_1^2 \partial X_2} + a_{13}\frac{\partial \Phi_{22}}{\partial X_2} = 0 \tag{9}$$

$$a_5\frac{\partial^3 U_1}{\partial X_1^2 \partial X_2} + a_6\frac{\partial U_1}{\partial X_2} + a_{11}\frac{\partial U_2}{\partial X_1} + a_{14}\frac{\partial^2 \Phi_{21}}{\partial X_1^2} + a_{15}\Phi_{21} = 0 \tag{10}$$

$$a_{12}\frac{\partial^3 U_2}{\partial X_1^2 \partial X_2} + a_{13}\frac{\partial U_2}{\partial X_2} + a_7\frac{\partial U_1}{\partial X_1} + a_{16}\frac{\partial^2 \Phi_{22}}{\partial X_1^2} + a_{17}\Phi_{22} = 0 \tag{11}$$

where $a_1 = \frac{(1+\eta)L_2^2(\lambda_2+2\mu_2)}{12}$, $a_2 = -\frac{\eta(\lambda_1+2\mu_1)+(\lambda_2+2\mu_2)}{(1+\eta)}$, $a_3 = -(1+\eta)\mu_2$, $a_4 = -(\lambda_2+\mu_2)$, $a_5 = -\frac{L_2^2\eta^2(\lambda_2+2\mu_2)}{12}$, $a_6 = \eta\mu_2$, $a_7 = -\frac{\eta(\lambda_1-\lambda_2)}{(1+\eta)}$, $a_8 = \frac{L_2^2(1+\eta)\mu_2}{12}$, $a_9 = -\frac{(\eta\mu_1+\mu_2)}{(1+\eta)}$, $a_{10} = -(1+\eta)(\lambda_2+2\mu_2)$, $a_{11} = -\frac{\eta(\mu_1-\mu_2)}{(1+\eta)}$, $a_{12} = -\frac{L_2^2\eta\mu_2}{12}$, $a_{13} = \eta(\lambda_2+2\mu_2)$, $a_{14} = \frac{L_2^2\eta^2[\eta(\lambda_1+2\mu_1)+(\lambda_2+2\mu_2)]}{12(1+\eta)}$, $a_{15} = -\frac{\eta(\mu_1+\eta\mu_2)}{(1+\eta)}$, $a_{16} = \frac{L_2^2\eta^2(\eta\mu_1+\mu_2)}{12(1+\eta)}$, $a_{17} = -\frac{\eta[(\lambda_1+2\mu_1)+\eta(\lambda_2+2\mu_2)]}{(1+\eta)}$, $\eta = \frac{L_1}{L}$.

The complete set of boundary conditions can be also obtained along the boundary parallel to the lamination. We have

$$t_j = \tau_{2j} + \sigma_{2j} - \frac{\partial \chi_{12j}}{\partial X_1} \tag{12}$$

in which t_j represents the simple surface traction, $\tau_{ij} = \frac{\partial W}{\partial e_{ij}}$ is Cauchy stress, $\sigma_{ij} = \frac{\partial W}{\partial \gamma_{ij}}$ is relative stress, and $\chi_{kij} = \frac{\partial W}{\partial \theta_{kij}}$ is couple stress. These form the complete constitutive relations for the microstructure medium that represents the original layered medium.

3 The crack problem in layered media

Consider a layered medium of infinite extent with a through-the-thickness crack of length 2a as shown in Fig. 2. The crack lies at $-a \le X_1 \le a$, $X_2 = 0$. The total unit cell length for the layered medium is denoted by $L = L_1 + L_2$. A uniform pressure p_0 is applied on the surfaces of the crack.

The microstructure continuum governed by Eqs. (8–11) is a macroscopically homogenous solid. For the crack problem, the boundary conditions at $X_2 = 0$ are:

$$t_2 = \tau_{22} + \sigma_{22} - \frac{\partial \chi_{122}}{\partial X_1} = -p_0 \quad \text{for } |X_1| < a \tag{13}$$

$$t_1 = \tau_{21} + \sigma_{21} - \frac{\partial \chi_{121}}{\partial X_1} = 0 \quad \text{for } |X_1| < a \tag{14}$$

$$U_2 = f_3(X_1), \quad f_3(X_1) = f_3(-X_1) \quad \text{for } |X_1| \le a \tag{15}$$

$$f_3(X_1) = 0 \quad \text{for } |X_1| \ge a \tag{16}$$

and the homogeneous far field conditions

$$t_j = 0 \quad \text{for } r = \sqrt{X_1^2 + X_2^2} \to \infty \tag{17}$$

To solve the problem, the exponential Fourier transform with respect to X_1 is used:

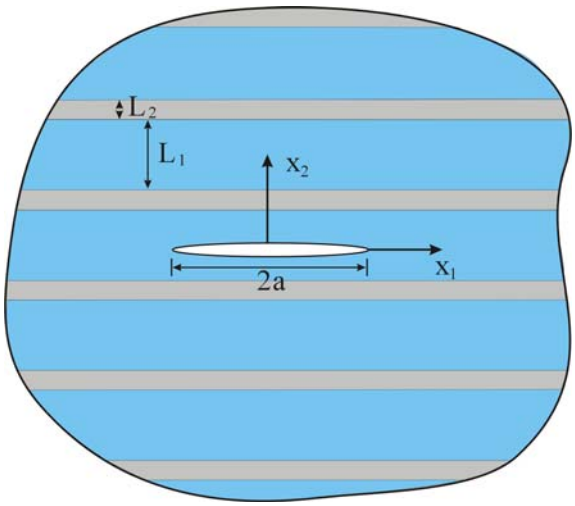

Fig. 2 An embedded through-the-thickness crack in a layered medium

$$\hat{f}(s) = \int_{-\infty}^{\infty} f(X_1) e^{isX_1} \mathrm{d}X_1,$$

$$f(X_1) = \frac{1}{2\pi} \int_{-\infty}^{\infty} \hat{f}(s) e^{-isX_1} \mathrm{d}s. \tag{18}$$

This method of solution consists in removing the X_1 dependence from the governing partial differential Equations (8)–(11) as well as from the boundary conditions. In this manner, the governing equations give rise to four ordinary differential equations as

$$\left(a_3 - a_1 s^2\right) \frac{\mathrm{d}^2 \hat{U}_1}{\mathrm{d}X_2^2} - a_2 s^2 \hat{U}_1 - isa_4 \frac{\mathrm{d}\hat{U}_2}{\mathrm{d}X_2} + \left(a_6 - a_5 s^2\right) \frac{\mathrm{d}\hat{\Phi}_{21}}{\mathrm{d}X_2} - isa_7 \hat{\Phi}_{22} = 0 \tag{19}$$

$$\left(a_{10} - a_8 s^2\right) \frac{\mathrm{d}^2 \hat{U}_2}{\mathrm{d}X_2^2} - a_9 s^2 \hat{U}_2 - isa_4 \frac{\mathrm{d}\hat{U}_1}{\mathrm{d}X_2} - isa_{11} \hat{\Phi}_{21} + \left(a_{13} - a_{11} s^2\right) \frac{\mathrm{d}\hat{\Phi}_{22}}{\mathrm{d}X_2} = 0 \tag{20}$$

$$\left(a_6 - a_5 s^2\right) \frac{\mathrm{d}\hat{U}_1}{\mathrm{d}X_2} - isa_{11} \hat{U}_2 + \left(a_{15} - a_{14} s^2\right) \hat{\Phi}_{21} = 0 \tag{21}$$

$$\left(a_{13} - a_{12} s^2\right) \frac{\mathrm{d}\hat{U}_2}{\mathrm{d}X_2} - isa_7 \hat{U}_1 + \left(a_{17} - a_{16} s^2\right) \hat{\Phi}_{22} = 0 \tag{22}$$

Eliminating $\hat{U}_1$, $\hat{\Phi}_{21}$ and $\hat{\Phi}_{22}$ using Eqs. (19)–(22), we obtain a single equation in $\hat{U}_2$:

$$B_1\frac{\mathrm{d}^4\hat{U}_2}{\mathrm{d}X_2^4}+B_2\frac{\mathrm{d}^2\hat{U}_2}{\mathrm{d}X_2^2}+B_3=0 \tag{23}$$

in which

$$\begin{aligned}
B_1&=\tilde{A}_1\tilde{B}_1,\\
B_2&=-(\tilde{A}_3\tilde{B}_3-\tilde{B}_1\tilde{A}_2-\tilde{B}_2\tilde{A}_1),\\
B_3&=\tilde{A}_2\tilde{B}_2\\
\tilde{A}_1&=\left(a_3-a_1s^2-\frac{(a_6-a_5s)^2}{a_{15}-a_{14}s^2}\right),\\
\tilde{A}_2&=-\left(a_2s^2-\frac{(a_7s)^2}{a_{17}-a_{16}s^2}\right)\\
\tilde{A}_3=\tilde{B}_3&=-is\left(a_4-a_{11}\frac{a_6-a_5s^2}{a_{15}-a_{14}s^2}-a_7\right.\\
&\qquad\left.\times\frac{a_{13}-a_{12}s^2}{a_{15}-a_{14}s^2}\right).\\
\tilde{B}_1&=\left(a_{10}-a_8s^2-\frac{\left(a_{13}-a_{12}s^2\right)^2}{a_{17}-a_{16}s^2}\right),\\
\tilde{B}_2&=-\left(a_9s^2-\frac{\left(a_{11}s^2\right)^2}{a_{15}-a_{14}s^2}\right).
\end{aligned}$$

The corresponding characteristic equation to the above ordinary differential equation is

$$B_1\lambda^4+B_2\lambda^2+B_3=0 \tag{24}$$

The four roots of the polynomial (24) above can be expressed as

$$\lambda_1=-\lambda_3,\lambda_2=-\lambda_4 \tag{25}$$

where $real\,(\lambda_1)<0$ and $real\,(\lambda_2)<0$. By taking account of the far field condition (17), we have

$$\hat{U}_2=\begin{cases}\alpha_1e^{\lambda_1X_2}+\alpha_2e^{\lambda_2X_2}, & X_2>0\\ \alpha_1e^{-\lambda_1X_2}+\alpha_2e^{-\lambda_2X_2}, & X_2<0\end{cases} \tag{26}$$

From Eqs. (19)–(22), the other displacement and micro deformation components are obtained as

$$\hat{U}_1=\begin{cases}D_1\alpha_1e^{\lambda_1X_2}+D_2\alpha_2e^{\lambda_2X_2}, & X_2>0\\ D_1\alpha_1e^{-\lambda_1X_2}+D_2\alpha_2e^{-\lambda_2X_2}, & X_2<0\end{cases} \tag{27}$$

$$\hat{\Phi}_{21}=\begin{cases}E_1\alpha_1e^{\lambda_1X_2}+E_2\alpha_2e^{\lambda_2X_2}, & X_2>0\\ E_1\alpha_1e^{-\lambda_1X_2}+E_2\alpha_2e^{-\lambda_2X_2}, & X_2>0\end{cases} \tag{28}$$

$$\hat{\Phi}_{22}=\begin{cases}F_1\alpha_1e^{\lambda_1X_2}+F_2\alpha_2e^{\lambda_2X_2}, & X_2>0\\ F_1\alpha_1e^{-\lambda_1X_2}+F_2\alpha_2e^{-\lambda_2X_2}, & X_2<0\end{cases} \tag{29}$$

where

$$\begin{aligned}
D_j&=\lambda_j\frac{\tilde{A}_1\left(\tilde{B}_2+\tilde{B}_1\lambda_j^2\right)-\tilde{A}_3\tilde{B}_3}{\tilde{A}_2\tilde{B}_3},\\
E_j&=-\lambda_j\frac{a_6-a_5s^2}{a_{15}-a_{14}s^2}D_j+\frac{isa_{11}}{a_{15}-a_{14}s^2},\\
F_j&=-\lambda_j\frac{a_{13}-a_{12}s^2}{a_{17}-a_{16}s^2}+\frac{isa_7}{a_{17}-a_{16}s^2}D_j,\quad j=1,2.
\end{aligned}$$

By using the boundary condition (13) and performing inverse Fourier transform and asymptotic analysis for the kernel function, the following governing equation is obtained

$$\begin{aligned}
&\frac{1}{2\pi}\int_{-a}^{a}f_3(u)\int_{-\infty}^{\infty}\left[\kappa_1(s)-b_7s^2-b_8\right]e^{-is(X_1-u)}\mathrm{d}s\mathrm{d}u\\
&\quad-b_7\frac{\mathrm{d}^2f_3(X_1)}{\mathrm{d}X_1^2}+b_8f_3(X_1)=-p_0
\end{aligned} \tag{30}$$

where the kernel function $\kappa_1(s)$ is a known function

$$\kappa_1(s)=\frac{\tilde{G}_1+\tilde{T}\tilde{G}_2+\tilde{L}_1+\tilde{T}\tilde{L}_2+is\tilde{T}\tilde{K}_2}{1+\tilde{T}} \tag{31}$$

with

$$\begin{aligned}
\tilde{G}_j&=\lambda_j\left(A_{2222}+\frac{1}{2}B_{2222}\right)-isA_{2211}D_j\\
&\quad-\frac{1}{2}B_{2222}F_j,\\
\tilde{L}_j&=\lambda_j\left(C_{2222}+\frac{1}{2}B_{2222}\right)-C_{2222}F_j\\
&\quad-\frac{1}{2}isB_{1122}D_j,\\
\tilde{K}_j&=-is\\
&\quad\left(F_{122122}\lambda_j+\left(\frac{1}{2}E_{122122}-F_{122122}\right)F_j\right),\\
\tilde{T}&=-\frac{\tilde{H}_1+\tilde{N}_1+is\tilde{M}_1}{\tilde{H}_2+\tilde{N}_2+is\tilde{M}_2},\\
\tilde{H}_j&=\lambda_j\left(A_{2112}+\frac{1}{2}B_{2121}\right)D_j-isA_{2112}\\
&\quad-\frac{1}{2}B_{2121}E_j,\\
\tilde{N}_j&=\lambda_j\left(C_{2121}+\frac{1}{2}B_{2121}\right)D_j-is\frac{1}{2}B_{2121}\\
&\quad-\frac{1}{2}C_{2121}E_j,\\
\tilde{M}_j&=-is\left(F_{121121}\lambda_jD_j\right.\\
&\quad\left.+\left(\frac{1}{2}E_{121121}-F_{121121}\right)E_j\right),\quad j=1,2,
\end{aligned}$$

$$A_{2222} = \eta\left(\lambda_1 + 2\mu_1\right) + (1-\eta)\left(\lambda_2 + 2\mu_2\right),$$
$$A_{2211} = \eta\lambda_1 + (1-\eta)\lambda_2,$$
$$A_{2112} = \eta\mu_1 + (1-\eta)\mu_2,$$
$$B_{2222} = 2\eta\left[-\left(\lambda_1 + 2\mu_1\right) + \left(\lambda_2 + 2\mu_2\right)\right],$$
$$B_{2121} = 2\eta\left(\mu_2 - \mu_1\right), \quad B_{1122} = 2\eta\left(\lambda_2 - \lambda_1\right),$$
$$C_{2222} = \left[\eta\left(\lambda_1 + 2\mu_1\right) + \frac{\eta}{(1-\eta)}\left(\lambda_2 + 2\mu_2\right)\right],$$
$$C_{2121} = \eta\left[\mu_1 + \frac{\eta}{(1-\eta)}\mu_2\right],$$
$$E_{122122} = \frac{L_2^2\mu_2}{6},$$
$$E_{121121} = \frac{L_2^2\left(\lambda_2 + 2\mu_2\right)}{6},$$
$$F_{122122} = \frac{L_2^2\mu_2}{12(1-\eta)},$$
$$F_{121121} = \frac{L_2^2\left(\lambda_2 + 2\mu_2\right)}{12(1-\eta)}.$$

and b_7 and b_8 are determined by conducting asymptotic analysis of the kernel function $\kappa_1(s)$ as $\lim_{|s|\to\infty}\kappa_1(s) = b_7 s^2 + b_8$, finally, the unknown functions $f_3(X_1)$ can be determined numerically by solving Eq. (30).

4 Numerical simulation

The collocation method and the Chebyshev polynomial expansion method are used to solve the integrodifferential Eq. (30). First, by introducing nondimensional variables

$$\bar{s} = sa, \quad \bar{u} = u/a, \quad \bar{X}_1 = X_1/a \tag{32}$$

in the governing equation, we have

$$\frac{1}{2\pi}\int_{-1}^{1} f_3(\bar{u}) \int_{-\infty}^{\infty}\left[\kappa_1(\bar{s}) - \frac{b_7}{a^2}\bar{s}^2 - b_8\right] e^{-i\bar{s}\left(\bar{X}_1 - \bar{u}\right)} \mathrm{d}\bar{s}\mathrm{d}\bar{u} - \frac{b_7}{a^2}\frac{d^2 f_3\left(\bar{X}_1\right)}{d\bar{X}_1^2} + b_8 f_3\left(\bar{X}_1\right) = -p_0 \tag{33}$$

Based on properties of the displacement field along the crack surface as given by (15), the approximation of function $f_3\left(\bar{X}_1\right)$ can be assumed by means of the Chebyshev polynomial expansion as

$$f_3\left(\bar{X}_1\right) = \sqrt{1-\bar{X}_1^2}\sum_{n=0}^{\infty}\tilde{E}_n U_n\left(\bar{X}_1\right) \tag{34}$$

in which U_n are Chebyshev polynomials of the second kind, and $\tilde{E}_n$ unknown constants to be determined. From (34), we have

$$\frac{d^2 f_3\left(\bar{X}_1\right)}{d\bar{X}_1^2} = \frac{n+1}{\left(1-\bar{X}_1^2\right)\sqrt{1-\bar{X}_1^2}}\sum_{n=0}^{\infty}\tilde{E}_n\left[n\bar{X}_1 T_{n+1}\left(\bar{X}_1\right) - (n+1)\,T_n\left(\bar{X}_1\right)\right] \tag{35}$$

where T_n are Chebyshev polynomials of the first kind.

If the expansion in (34) is truncated at the Nth term and Eq. (33) is satisfied at the following collocation points along the length of the crack

$$\bar{X}_1^{(l)} = \cos\left(\frac{l}{N+1}\pi\right), \quad l = 1, 2, \ldots, N \tag{36}$$

then N linear algebraic equations in terms of $\{d\} = \left\{\tilde{E}_1, \tilde{E}_2, \ldots, \tilde{E}_N\right\}$ are obtained as

$$[Q]\{d\} = \{t\} \tag{37}$$

where $[Q]$ is a known $N \times N$ matrix given in Appendix. The general loading $\{t\} = \left\{t^{(1)}, t^{(2)}, \ldots, t^{(N)}\right\}$ used in Eq. (37) is given as

$$t^{(l)} = -p_0, \quad l = 1, 2, \ldots, N \tag{38}$$

Based on the obtained solution $\{d\}$ in Eq. (37), the normal component of the traction along $\bar{X}_2 = 0$, $\left|\bar{X}_1\right| > 1$, is obtained as

$$t_2 = \frac{1}{2\pi}\int_{-1}^{1} f_3(\bar{u}) \int_{-\infty}^{\infty}\left[\kappa_1(\bar{s}) - \frac{b_7}{a^2}\bar{s}^2 - b_8\right] e^{-i\bar{s}\left(\bar{X}_1 - \bar{u}\right)} \mathrm{d}\bar{s}\mathrm{d}\bar{u} \tag{39}$$

From the expression above, it is noted that there exists no stress singularity at the crack tip because no singular term appears in the integral.

5 Numerical results and discussion

Numerical solutions for the layered medium with an embedded parallel crack as shown in Fig. 2 are carried out. The main purpose of these numerical solutions is to make comparisons among the three solutions: the finite element solution based on the exact layered geometry, the effective modulus theory which treats the layered medium as a classical anisotropic solid, and the present

microstructure continuum theory. Through these comparisons it is our hope to better understand the meaning of the use of the microstructure continuum theory in modeling crack problems in heterogeneous media.

5.1 Crack opening displacement

Figure 3 shows the comparison of the normalized displacement along the crack surface U_2/a calculated from Eq. (34). The crack surfaces are under a uniform pressure $p_0/\mu_2 = 1$. The material constants and geometrical parameters are assumed to be $L_1/L_2 = 4$, $\mu_1/\mu_2 = 50$, $v_1 = 0.3$ and $v_2 = 0.35$. The position of the crack is assumed to be at the mid-plane of a layer of material 1. The corresponding "exact" solution is obtained using the commercial finite element code ANSYS to analyze the original cracked layered medium. Two-dimensional plane element (four nodes 'PLANE182', plane strain option) is chosen to model the layered medium. Fine meshes around the crack tips are used to obtained converged solutions. The solution of the effective modulus theory (i.e., the layered medium is represented by an equivalent homogenous orthotropic solid) is also included for comparison (Sih and Liebowitz 1968). The results in Fig. 3 indicate that for layered media with large crack lengths relative to the microstructure dimension, L, both the microstructure continuum and the effective modulus theory yield pretty accurate crack opening displacement. The results also show that the crack opening displacement is significantly influenced by the L/a ratio. It is noted that the effective modulus theory becomes inaccurate when the length ratio L/a increases while the microstructure continuum theory is reasonably accurate up to $L/a = 1$.

Figure 4 shows a similar comparison of the normalized crack opening displacements for the layered medium with $L_1/L_2 = 4$, $\mu_1/\mu_2 = 10$, $v_1 = 0.3$ and $v_2 = 0.35$. The position of the crack is assumed to be at the same position as that in Fig. 3. Similar trends are observed. However, the microstructural effect on the crack opening is not so significant as compared with the results in Fig. 3.

It is expected that there is a substantial difference between placing a crack in the stiff layer and in the soft layer. For this reason, we consider now a crack lying at the middle plane of a softer layer in the layered medium. The material properties are set as $L_1/L_2 = 0.25$, $\mu_1/\mu_2 = 0.1$, $v_1 = 0.35$ and $v_2 = 0.3$. The applied pressure is kept to be $p_0/\mu_2 = 1$. Figure 5 clearly shows that, in this case, the variation of L/a ratio does not have much influence on the crack opening displacement and the microstructure continuum theory is adequate for L/a ratios not too close to unity. Based on the numerical solutions obtained, it seems that better predictions can be obtained by using the microstructure continuum theory if the crack lies in the stiffer layer and that if the stiffness ratio μ_1/μ_2 is large.

When the crack is located at an arbitrary position in the layered medium, the symmetric condition between the two crack surfaces can not be satisfied. In fact, this type of local asymmetry is very difficult if not impossible to model with an equivalent homogeneous medium.

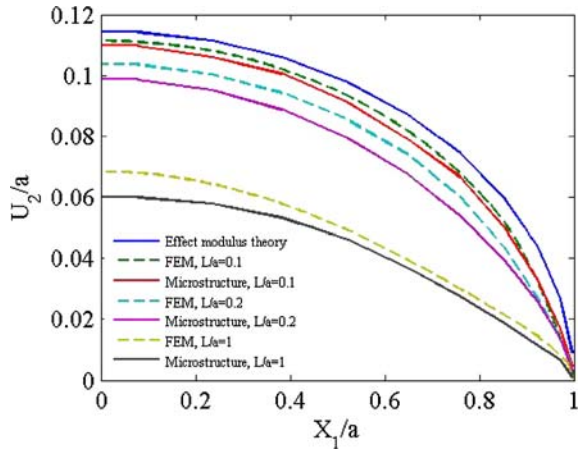

Fig. 3 Normalized crack opening displacement for a horizontal crack located in a stiff layer with $\mu_1/\mu_2 = 50$ and $p_0/\mu_2 = 1$

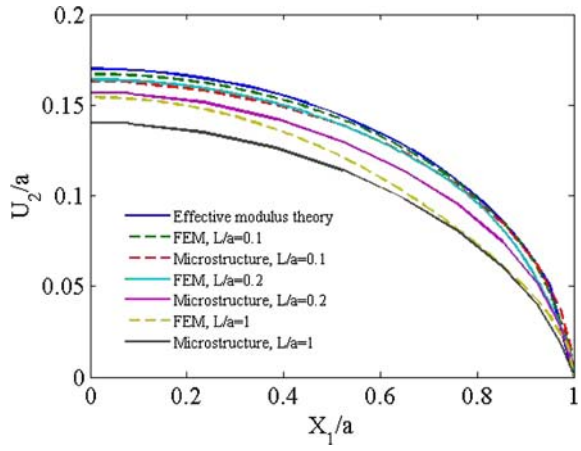

Fig. 4 Normalized crack opening displacement for a horizontal crack located in a stiff layer with $\mu_1/\mu_2 = 10$ and $p_0/\mu_2 = 1$

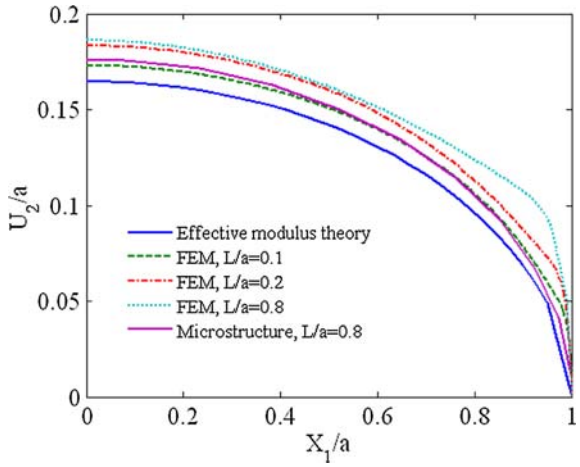

Fig. 5 Normalized crack opening displacement for a horizontal crack located in a soft layer with $\mu_1/\mu_2 = 0.1$ and $p_0/\mu_2 = 1$

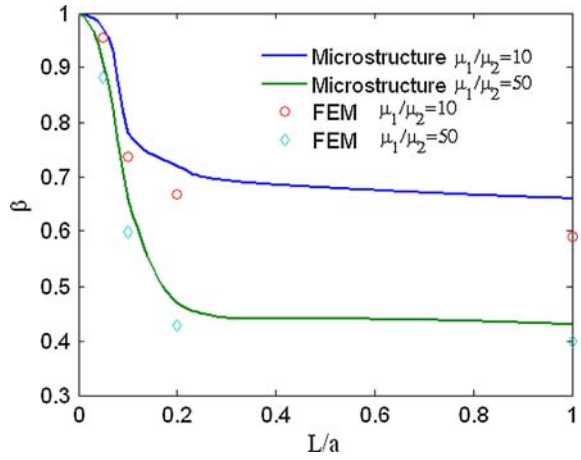

Fig. 6 Normalized stress distribution around the tip of the parallel crack

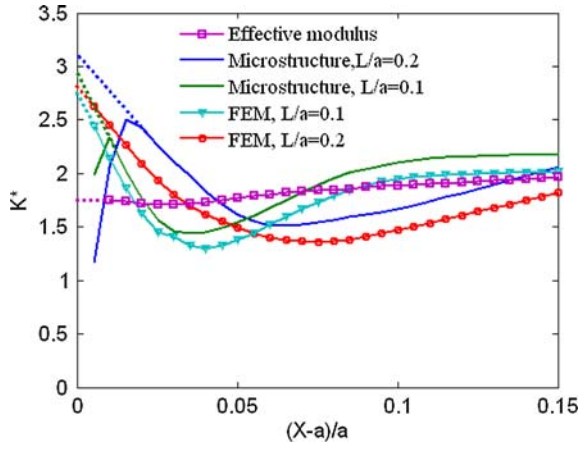

Fig. 7 Normalized stress intensity factor for $\mu_1/\mu_2 = 10$ and $p_0/\mu_2 = 1$

5.2 Crack tip stress fields

Based on the present microstructure continuum theory, there does not exist a singular deformation field near the crack tip according to Eq. (39). This behavior is different from that in elastic solids. In this subsection we numerically compare the crack tip stress field predicted by the microstructure continuum theory and that calculated using the FEA in conjunction with the exact layered geometry. The FEA result is regarded as the "exact" solution. The comparison is made based on the ratio $\beta = \lim_{\bar{X}_1 - 1 \to 0.01} \left[\frac{\overset{o}{t}_2(\bar{X}_1, 0)}{t_2(\bar{X}_1, 0)} \right]$ where $\overset{o}{t}_2\left(\overline{X}_1, 0\right)$ is the crack opening stress according to the solution of the effective modulus medium at a distance of $0.01a$ from the crack tip (the solution can be found in Sih and Liebowitz 1968), and $t_2\left(\bar{X}_1, 0\right)$ is the normal component of the Cauchy stress (given by Eq. 39) from the microstructure continuum theory or the finite element analysis of the exact layered medium. Two layered media with $\mu_1/\mu_2 = 10$ and $\mu_1/\mu_2 = 50$, respectively, are considered. The comparison presented in Fig. 6 indicates that the microstructure continuum theory can give fairly accurate opening stress near the crack tip for the range up to $L/a = 1$. It is noted that, as $L/a \to 0$, the microstructure continuum solution converges to its classical continuum (effective modulus theory) counterpart. Hence, theoretically, the near tip stress field on the microstructure continuum theory would become singular as $L/a \to 0$ (Fig. 6).

It is a popular approach in fracture mechanics of linear elastic solids to determine the stress intensity factor numerically by plotting the opening stress versus the distance from the crack tip in the form $K = t_2\sqrt{2\pi(X_1 - a)}$. The stress intensity factor is obtained as X_1 approaches a, the crack tip location. Although the opening stress t_2 according to the microstructure continuum theory is not singular, we also plot $K = t_2\sqrt{2\pi(X_1 - a)}$ for comparison. In Fig. 7, normalized "stress intensity factors" $K^* = K/p_0\sqrt{a}$ for the layered medium with $L_1/L_2 = 4$, $\mu_1/\mu_2 = 10$, $\upsilon_1 = 0.3$ and $\upsilon_2 = 0.35$ obtained with the microstructure continuum theory, the finite element method, and the effective modulus theory are shown. It is evident that the stress intensity factor according to the microstructure continuum theory diminishes as X_1 approaches

a (the crack tip) that is consistent with the fact that the opening stress is not singular. If we ignore the last portion of the curve and project the value of K^*(at $X_1 = a$) as shown by the dashed line, then the FEM solutions and the microstructure continuum solutions are in fairly good agreement. On the other hand, the stress intensity factor by the effective modulus theory is not influenced by the ratio L/a and appears to be substantially lower than those obtained with the FEM. It is noted that the decrease of $K^* = K/p_0\sqrt{a}$ according to the microstructure continuum theory does not mean that the opening stress obtained from the microstructure continuum theory decreases when approaching the crack tip. In fact, the opening stress increases but remains bounded as $(X_1 - a)$ approaches zero. This result indicate that the present microstructure continuum theory cannot accurately describe the local singular stress field with high strain gradient. It is expected that a higher order microstructure continuum theory should be able to yield more accurate local stresses near the crack tip. Nevertheless, the result in Fig. 7 indicates that a reasonable estimation of the local stress intensity factor may be obtained using the projection method based on the stress field of the microstructure continuum at a short distance from the crack tip.f.

6 Conclusions

In this study, a microstructure continuum theory was employed to analyze crack opening stresses in a 2D layered medium consisting of two different alternating elastic materials. For the crack was assumed to be parallel to the plane of the layer and subjected to a uniform pressure on the crack surfaces. Fourier transform was employed to solve the problem. The resulting integrodifferential equations were discretized using the collocation method and the Chebyshev method. It was found that the microstructure continuum solution yielded no stress singular near the crack tip. Numerical solutions showed that the effective modulus theory for the layered medium tends to overestimate the crack opening displacement and the crack opening stress near the crack tip if the crack is located in the stiff layer. The converse is true if the crack is located in a soft layer. Finally, the local stress intensity factor obtained using a projection technique based on the microstructure continuum solution was found to be in fairly good agreement with the finite element solution based on the exact layered geometry.

Appendix

The matrix $[Q]$ used in Eq. (37) is given by

$$Q = \begin{bmatrix} Q_{11} & Q_{12} & \cdots & Q_{1N} \\ Q_{21} & Q_{22} & \cdots & Q_{2N} \\ \vdots & \vdots & \vdots & \vdots \\ Q_{N1} & \cdots & \cdots & Q_{NN} \end{bmatrix}$$

with

$$Q_{nl} = \frac{1}{2\pi}\int_{-1}^{1}\sqrt{1-\bar{u}^2}u_n(\bar{u})\int_{-\infty}^{\infty}\left[\kappa(\bar{s}) - \frac{b_7}{a^2}\bar{s}^2 - b_8\right]e^{-i\bar{s}\left(\bar{X}_1^{(l)}-\bar{u}\right)}\mathrm{d}\bar{s}\mathrm{d}\bar{u}$$
$$-\frac{b_7}{a^2}\frac{n+1}{\left(1-\left(\bar{X}_1^{(l)}\right)^2\right)\sqrt{1-\left(\bar{X}_1^{(l)}\right)^2}^2}$$
$$\times\left[n\bar{X}_1^{(l)}T_{n+1}\left(\bar{X}_1^{(l)}\right) - (n+1)\,T_n\left(\bar{X}_1^{(l)}\right)\right] + b_8\sqrt{1-\left(\bar{X}_1^{(l)}\right)^2}^2 U_n\left(\bar{X}_1^{(l)}\right)$$

$n, l = 1, 2, \ldots, N.$

References

Achenbach JD, Sun CT, Herrmann G (1968) On the vibrations of a laminated body. J Appl Mech 35:689–696

Aifantis EC (1999) Gradient deformation models at nano, micro, and macro scales. ASME J Eng Mater Tech 121:189–202. doi:10.1115/1.2812366

Atkinson C, Leppington FG (1977) The effect of couple stress on the tip of a crack. Int J Solids Struct 13:1103–1122. doi:10.1016/0020-7683(77)90080-4

Cosserat E, Cosserat F (1909) Theorie des Corps Deformables. A. Hermann & Fils, Paris

Eringen AC, Speziale CG, Kim BS (1977) Crack tip problem in non-local theory. J Mech Phys Solids 25:339–355. doi:10.1016/0022-5096(77)90002-3

Eringen AC, Suhubi ES (1964) Nonlinear theory of micro-elastic solids. Int J Eng Sci 2:189–203. doi:10.1016/0020-7225(64)90004-7

Fannjiang AC, Chan YS, Paulino GH (2002) Strain gradient elasticity for antiplane shear cracks: a hypersingular integrodifferential equation approach. SIAM J Appl Math 62:1066–1091. doi:10.1137/S0036139900380487

Fleck N, Hutchinson J (1993) A phenomenological theory for strain gradient effects in plasticity. J Mech Phys Solids 41:1825–1857. doi:10.1016/0022-5096(93)90072-N

Huang Y, Zhang L, Guo TF, Hwang KC (1997) Mixed mode near-tip fields for cracks in materials with strain-gradient effects. J Mech Phys Solids 45:439–465. doi:10.1016/S0022-5096(96)00089-0

Kennedy TC, Kim JB (1993) Dynamic analysis of cracks in micropolar elastic materials. Eng Fract Mech 44:207–216. doi:10.1016/0013-7944(93)90045-T

Mindlin RD (1964) Micro-structure in linear elasticity. Arch Ration Mech Anal 16:51–78. doi:10.1007/BF00248490

Paul HS, Sridharan K (1981) The problem of a griffith crack in micropolar elasticity. Int J Eng Sci 19:563–579. doi:10.1016/0020-7225(81)90090-2

Sih GC, Liebowitz H (1968) . In: Liebowitz H (ed) Fracture: an advanced treatise, vol 2. Academic Press, New York, pp 67–190

Sternberg E, Muki R (1967) The effect of couple-stress on the stress concentration around a crack. Int J Solids Struct 3:69–95. doi:10.1016/0020-7683(67)90045-5

Sun CT, Achenbach JD, Herrmann G (1968) Continuum theory for a laminated medium. J Appl Mech 35:467–475

Toupin RA (1962) Elastic materials with couple-stresses. Arch Ration Mech Anal 11:385–414. doi:10.1007/BF00253945

Vardoulakis I, Exadaktylos G, Aifantis E (1996) Gradient elasticity with surface energy: mode-III crack problem. Int J Solids Struct 33:4531–4559. doi:10.1016/0020-7683(95)00277-4

Zhang L, Huang Y, Chen JY, Hwang KC (1998) The mode III full-field in elastic materials with strain gradient effects. Int J Fract 92:325–348. doi:10.1023/A:1007552621307